Hindawi Publishing Corporation
Shock and Vibration
Volume 2016, Article ID 2689178, 14 pages
http://dx.doi.org/10.1155/2016/2689178

Research Article

Modelling and Composite Control of Single Flexible Manipulators with Piezoelectric Actuators

En Lu,[1] Wei Li,[1] Xuefeng Yang,[1] Mengbao Fan,[1] and Yufei Liu[1,2]

[1]*School of Mechatronic Engineering, China University of Mining and Technology, Xuzhou 221116, China*
[2]*School of Mechanical and Automotive Engineering, Anhui Polytechnic University, Wuhu 241000, China*

Correspondence should be addressed to Wei Li; liweicumt@163.com

Received 11 July 2016; Accepted 23 August 2016

Academic Editor: Salvatore Russo

The piezoelectric actuators are used to investigate the active vibration control of flexible manipulators in this paper. Based on the assumed mode method, piezoelectric coupling model, and Hamilton's principle, the dynamic equation of the single flexible manipulator (SFM) with surface bonded actuators is established. Then, a singular perturbation model consisted of a slow subsystem and a fast subsystem is formulated and used for designing the composite controller. The slow subsystem controller is designed by fuzzy sliding mode control method, and the linear quadratic regulator (LQR) optimal control method is used to design fast subsystem controller. Furthermore, the changing trends of natural frequencies along with the changes in the position of piezoelectric actuators are obtained through the ANSYS Workbench software, by which the optimal placement of actuators is determined. Finally, numerical simulations and experiments are presented. The results demonstrate that the method of optimal placement is feasible based on the maximal natural frequency, and the composite controller presented in this paper can not only realize the trajectory tracking of the SFM and has a good result on the vibration suppression.

1. Introduction

In recent years, the robotic technology has been widely used in many areas, such as aerospace, industry, and medical treatment. Due to the characteristics of high speed, high precision, and high loading weight ratio, flexible structures have received great attention in the robot areas [1, 2]. The elastic deformations of flexible manipulators couple with the rigid motions of rigid bodies in the light-duty and high-speed flexible manipulators system [1], and they have obvious influence on the positioning precision of the equipment. Therefore, lots of scholars have done tons of researches on the vibration suppression of flexible manipulators. Smart piezoelectric material, especially the piezoelectric ceramic, has a superior characteristic of dual functions of actuating and sensing with excellent mechanical-electrical coupling characteristics which are widely used in the study of active vibration control of flexible manipulators [3].

The dynamical model of flexible manipulators has the features of being time-varying, strong coupling, and highly nonlinear which brings insuperable difficulties of the single controller design and it is hard to get ideal control effect [4]. Besides, the trajectory tracking and vibration suppression of flexible manipulators need to be controlled at the same time during movement. Therefore, to realize the trajectory tracking and vibration suppression while simplifying the design of controller and improving the robustness properties, the singular perturbation theory has been shown to be a convenient strategy for "reduced-order modelling" in recent years [5]. Based on the singular perturbation theory, the highly nonlinear and strongly coupled dynamic equation of flexible manipulators is decomposed into a slow subsystem corresponding to the rigid body and a fast subsystem describing the flexible motion. Then according to the characteristics of the two subsystems, the controllers are designed independently. For example, Siciliano and Book [4] proposed a state feedback controller based on the singular perturbation model of single flexible manipulator (SFM), and the trajectory tracking and vibration suppression was realized through the way of controlling the motor torque. Analogously, singular perturbation adaptive controller of multiple flexible links manipulators was designed by Yu and Chen [6]. Lin and

Lewis [5] carried on the control simulations of flexible link robot arms and the control torque was obtained through two-time scale fuzzy logic controller. Computed torque control and a composite control were utilized to reduce mechanical vibrations of SFM by Jia et al. [7]. In the composite control system, a dynamic sliding mode controller was designed for slow subsystem, and optimal controller was designed for fast subsystem. From the above it can be seen that all the active vibration controls of flexible manipulators were realized by the way of controlling the motor torque, and most scholars less focused on the composite control of SFM with piezoelectric actuators based on the singular perturbation theory.

Moreover, experiments and simulations results have proved that the positions of the actuators have important influence on vibration suppression effect [8], and the research hotspots focus on the optimal criterion and solution algorithm. Qiu et al. [9] and Leleu et al. [10] have conducted research on the control indexes of open-loop control system based on controllability and observability. The performance indexes of the closed-loop control system were studied from the angle of the control energy and vibration energy [11–13]. After establishing optimal criterion, many intelligent search algorithms such as genetic algorithm, particle swarm optimization algorithm, and ant colony algorithm can be applied to solve the optimal problem of actuators or sensors. When the size or number of piezoelectric actuators and sensors reaches a certain extent, the natural frequencies of flexible manipulators will be changed and the system stability is reduced. Zhang et al. [14] analyzed the natural frequencies of a piezoelectric beam by the general finite element software ANSYS, the modal frequencies of the system are changed at a certain extent, and the change of modal frequencies explains that the piezoelectric actuators have some influence on the natural frequencies of the host structure. Therefore, it is necessary to analyze the effect of the piezoelectric actuators or sensors which are bonded on flexible manipulators. Abreu et al. [15] researched the influence of the position of piezoelectric actuators on the natural frequencies by experiment method. Waisman and Abramovich [16] investigated the influence of the actuators by means of the pin-force model, and numerical experiments demonstrate that the natural frequencies and vibration modes of the structure can be actively altered using the piezoelectric actuators. Spier et al. [17] analyzed the locations of actuators and sensors with the fundamental frequency and the frequency gaps between the higher order frequencies. A review of the literature reveals that the actuators or sensors can change the structural characteristics of flexible manipulators. Therefore, the location of optimization of piezoelectric actuator based on the index of natural frequency is useful to avoid resonance when the excitation frequency is around the natural frequency. However, many scholars tend to neglect this in the study of optimal placement of actuators or sensors.

This paper aims to investigate the modelling and composite control of the SFM with piezoelectric actuators and realizes the trajectory tracking and vibration suppression of flexible manipulators based on the composite controller which is designed by singular perturbation theory. Furthermore, the optimal placement of piezoelectric actuators is done through the index of the maximal natural frequency. The paper is organized as follows: "Dynamic Model of the SFM" is illuminated in the following section. "Singular Perturbation Decomposition of Dynamic Equation" presents the reduction of dynamic equation. Subsequently, a compound controller is designed for trajectory tracking and vibration suppression of the SFM in "Design of the Composite Controller" of this paper. Then, the location optimization of piezoelectric actuators, simulation, and experiments results of the composite control method are given in "Optimal Placement and Composite Control of the SFM." The paper is concluded with a brief summary in last section.

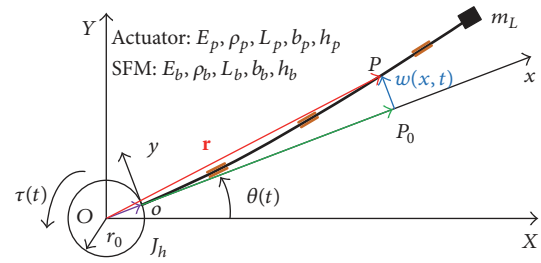

Figure 1: Structural diagram of the SFM.

2. Dynamic Model of the SFM

The structural diagram of the SFM in the horizontal plane studied in this paper is shown in Figure 1 and two actuators which are dual surface bonded on the SFM are denoted as a group. The specifications of the actuators are chosen to be the same and they are made of piezoelectric ceramic. In the figure, the coordinates XY and xy indicate the inertial frame and the reference frame, respectively. And $\tau(t)$ is the output torque of the speed reducer which is driven by a motor, J_h is the rotational inertia of the hub (motor shaft and fixture), r is the radius of the hub, $\theta(t)$ is the angular displacement of the hub, and m_L is the tip mass of the SFM. Besides, E_b, ρ_b, L_b, b_b, and h_b denote the elastic modulus, density, length, width of cross section, and height of cross section of the SFM, respectively. E_p, ρ_p, L_p, b_p, and h_p denote the elastic modulus, density, length, width of cross section, and height of cross section of the actuators, respectively.

As shown in Figure 1, the position vector of point P with respect to the reference frame xy can be represented as [18]

$$\mathbf{r} = \mathbf{\Theta} \begin{bmatrix} r_0 + x \\ w(x,t) \end{bmatrix}, \tag{1}$$

$$\mathbf{\Theta} = \begin{bmatrix} \cos\theta & -\sin\theta \\ \sin\theta & \cos\theta \end{bmatrix}, \tag{2}$$

where $\mathbf{\Theta}$ is the rotational transformation matrix and $w(x,t)$ represents the transversal deformation of the SFM.

The velocity vectors of point P can be obtained by (1) as follows:

$$\dot{\mathbf{r}} = \dot{\mathbf{\Theta}} \begin{bmatrix} r_0 + x \\ w(x,t) \end{bmatrix} + \mathbf{\Theta} \begin{bmatrix} 0 \\ \dot{w}(x,t) \end{bmatrix}. \tag{3}$$

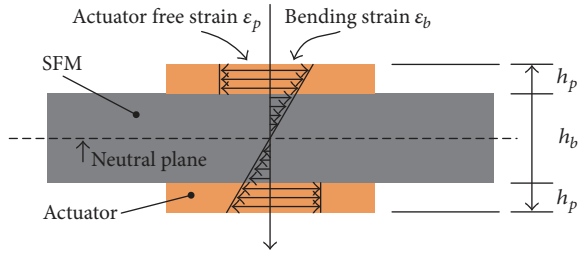

FIGURE 2: Model of the SFM with surface bonded actuators.

The kinetic energy of the SFM is written as

$$T = \frac{1}{2}J_h\dot{\theta}^2 + \frac{1}{2}\int_0^L \rho_b A_b \dot{\mathbf{r}}^T \dot{\mathbf{r}}\, dx + \frac{1}{2}\sum_{i=1}^{n}\int_{a_{i1}}^{a_{i2}} \rho_p A_p \dot{\mathbf{r}}^T \dot{\mathbf{r}}\, dx + \frac{1}{2}m_L \dot{\mathbf{r}}_L{}^T \dot{\mathbf{r}}_L, \tag{4}$$

where $\mathbf{r}_L$ is the coordinate of the position vector from O to the tip mass, a_{i1} is the starting position of the ith actuator, and a_{i2} is the ending position of the ith actuator.

Based on Euler–Bernoulli theory, the potential energy is given by

$$V = \frac{1}{2}\int_0^L E_b I_b \left(\frac{\partial^2 w(x,t)}{\partial x^2}\right)^2 dx + \frac{1}{2}\sum_{i=1}^{n}\int_{a_{i1}}^{a_{i2}} E_p I_p \left(\frac{\partial^2 w(x,t)}{\partial x^2}\right)^2 dx. \tag{5}$$

As shown in Figure 2, for the model of the SFM with surface bonded actuators, cross section strain distribution along the thickness is linear and using Hooke's law to obtain an expression for stress in terms of strain:

$$\sigma_b = E_b\varepsilon_b = E_b\frac{1}{\rho}y,$$
$$\sigma_P = E_P\left(\varepsilon_b - \varepsilon_p\right) = E_P\left(\frac{1}{\rho}y - \left(\frac{d_{31}}{h_p}\right)\mathbf{U}_i\right), \tag{6}$$

where ρ is the curvature radius of the neutral layer and y is the distance from the neutral plane.

Because the model is symmetrical, taking the upper part of the SFM with surface bonded actuators as an example to empirical analysis and the moment equilibrium equation about the neutral plane is given as [19]

$$\int_0^{h_b/2} y\sigma_b\, dy + \int_{h_b/2}^{h_b/2+h_p} y\sigma_p\, dy = 0,$$
$$\frac{1}{\rho} = \frac{E_p\left(12h_bh_p + 12h_p^2\right)\left(d_{31}/h_p\right)\mathbf{U}_i}{E_b{h_b}^3 + E_p\left(6{h_b}^2h_p + 12h_b{h_p}^2 + 8{h_p}^3\right)}. \tag{7}$$

The bending moment of the ith actuator can be determined using (12):

$$M_i = \left(E_bI_b + 2E_pI_p\right)\frac{1}{\rho} = \frac{\left(E_b{h_b}^3b_b + 2E_p{h_p}^3b_p\right)E_p\left(h_bh_p + {h_p}^2\right)\left(d_{31}/h_p\right)}{E_b{h_b}^3 + E_p\left(6{h_b}^2h_p + 12h_b{h_p}^2 + 8{h_p}^3\right)} \cdot \mathbf{U}_i(t) = \kappa\mathbf{U}_i(t), \tag{8}$$

where

$$\kappa = \frac{\left(E_b{h_b}^3b_b + 2E_p{h_p}^3b_p\right)E_p\left(h_bh_p + {h_p}^2\right)\left(d_{31}/h_p\right)}{E_b{h_b}^3 + E_p\left(6{h_b}^2h_p + 12h_b{h_p}^2 + 8{h_p}^3\right)}. \tag{9}$$

The virtual work carried out by the torque $\tau(t)$ and actuators acting on the SFM can be represented by [20]

$$\delta W = \tau(t)\,\delta\theta + \sum_{i=1}^{n}\kappa\mathbf{U}_i(t)\,\delta\theta + \sum_{i=1}^{n}\kappa\mathbf{U}_i(t)\left(\dot{\mathbf{\Phi}}(a_{i2}) - \dot{\mathbf{\Phi}}(a_{i1})\right)\delta\dot{\mathbf{q}}, \tag{10}$$

where $\kappa\mathbf{U}_i(t)$ is a bending moment generated by the ith actuator. κ is a positive constant representing the bending moment per volt. $\mathbf{U}_i(t)$ is the control voltage applied to the ith actuator. The term $(\dot{\mathbf{\Phi}}(a_{i2}) - \dot{\mathbf{\Phi}}(a_{i1}))\delta\dot{\mathbf{q}}$ denotes the slope difference between two ends of the ith actuator. For simplicity, we define $\dot{\mathbf{\Phi}}(a_{i2}) - \dot{\mathbf{\Phi}}(a_{i1}) = \widetilde{\dot{\mathbf{\Phi}}}(i)$.

In accordance with the assumed mode method, $w(x,t)$ is written as

$$w(x,t) = \sum_{i=1}^{\infty}\phi_j(x)\,q_j(t), \tag{11}$$

where $\phi_j(x)$ is the jth mode shapes and $q_j(t)$ is the jth mode generalized coordinates.

The governing equation of motion can be obtained through the application of the Hamilton's principle

$$\int_{t_0}^{t_f}(\delta T - \delta V + \delta W)\,dt = 0. \tag{12}$$

By substituting (4), (5), and (10) into (12), the dynamics equation of the SFM at the element level in compact form can be written as

$$\begin{bmatrix} M_{\theta\theta}(\theta,\mathbf{q}) & \mathbf{M}_{\theta q}(\theta,\mathbf{q}) \\ \mathbf{M}_{q\theta}(\theta,\mathbf{q}) & \mathbf{M}_{qq}(\theta,\mathbf{q}) \end{bmatrix}\begin{bmatrix}\ddot{\theta}\\ \ddot{\mathbf{q}}\end{bmatrix} + \begin{bmatrix} h_{\theta\theta}(\theta,\mathbf{q},\dot{\theta},\dot{\mathbf{q}}) & \mathbf{h}_{\theta q}(\theta,\mathbf{q},\dot{\theta},\dot{\mathbf{q}}) \\ \mathbf{h}_{q\theta}(\theta,\mathbf{q},\dot{\theta},\dot{\mathbf{q}}) & \mathbf{h}_{qq}(\theta,\mathbf{q},\dot{\theta},\dot{\mathbf{q}}) \end{bmatrix}\begin{bmatrix}\dot{\theta}\\ \dot{\mathbf{q}}\end{bmatrix} + \begin{bmatrix} 0 & \mathbf{0} \\ \mathbf{0} & \mathbf{K}_{qq} \end{bmatrix}\begin{bmatrix}\theta\\ \mathbf{q}\end{bmatrix} = \begin{bmatrix}\tau(t) + \mathbf{g}_\theta\mathbf{U} \\ \mathbf{g}_q\mathbf{U}\end{bmatrix}, \tag{13}$$

where

$$
\begin{aligned}
M_{\theta\theta} &= J_h + \frac{1}{3}\rho_b A_b\left[(r+L)^3 - r^3\right] + \frac{1}{3}\\
&\cdot \sum_{i=1}^{n}\rho_p A_P\left[\left(r+a_{i2}\right)^3 - \left(r+a_{i1}\right)^3\right] + \mathbf{q}^T\mathbf{M}_{ff}\mathbf{q}\\
&+ m_L\left(r+L\right)^2,\\
\mathbf{M}_{\theta q} &= \int_0^L \rho_b A_b\left(r_0+x\right)\mathbf{\Phi}\left(x\right)dx\\
&+ \sum_{i=1}^{n}\int_{a_{i1}}^{a_{i2}}\rho_p A_P\left(r_0+x\right)\mathbf{\Phi}\left(x\right)dx + m_L\left(r_0+L\right)\\
&\cdot \mathbf{\Phi}\left(L\right),\\
\mathbf{M}_{q\theta} &= \left[\mathbf{M}_{\theta q}\right]^{-1},\\
\mathbf{M}_{qq} &= \int_0^L \rho_b A_b \mathbf{\Phi}\left(x\right)^T\mathbf{\Phi}\left(x\right)dx\\
&+ \sum_{i=1}^{n}\int_{a_{i1}}^{a_{i2}}\rho_p A_P\mathbf{\Phi}\left(x\right)^T\mathbf{\Phi}\left(x\right)dx + m_L\mathbf{\Phi}^T\left(L\right)\mathbf{\Phi}\left(L\right),\\
h_{\theta\theta} &= 2\dot{\mathbf{q}}^T\mathbf{M}_{qq}\mathbf{q},\\
\mathbf{h}_{\theta q} &= \dot{\theta}\mathbf{q}^T\mathbf{M}_{qq},\\
\mathbf{h}_{q\theta} &= -\mathbf{M}_{qq}\mathbf{q}\dot{\theta},\\
\mathbf{h}_{qq} &= 0,\\
\mathbf{K}_{qq} &= \int_0^L E_b I_b\ddot{\mathbf{\Phi}}^T\left(x\right)\ddot{\mathbf{\Phi}}\left(x\right)dx\\
&+ \sum_{i=1}^{n}\int_{a_{i1}}^{a_{i2}}E_p I_P\ddot{\mathbf{\Phi}}^T\left(x\right)\ddot{\mathbf{\Phi}}\left(x\right)dx,\\
\mathbf{g}_\theta &= \kappa\left[1 \ \cdots \ 1\right],\\
\mathbf{g}_q &= \kappa\left[\widetilde{\dot{\mathbf{\Phi}}}\left(1\right) \ \cdots \ \widetilde{\dot{\mathbf{\Phi}}}\left(n\right)\right].
\end{aligned}
\tag{14}
$$

3. Singular Perturbation Decomposition of Dynamic Equation

Since the inertia matrix $\mathbf{M}$ in (13) is positively definite, it can be inverted and denoted by $\mathbf{N}$, which can be partitioned [7].

$$
\begin{aligned}
\mathbf{N}\left(\theta,\mathbf{q}\right) &= \begin{bmatrix} N_{\theta\theta}\left(\theta,\mathbf{q}\right) & \mathbf{N}_{\theta q}\left(\theta,\mathbf{q}\right)\\ \mathbf{N}_{q\theta}\left(\theta,\mathbf{q}\right) & \mathbf{N}_{qq}\left(\theta,\mathbf{q}\right)\end{bmatrix} = \mathbf{M}^{-1}\\
&= \begin{bmatrix} M_{\theta\theta} & \mathbf{M}_{\theta q}\\ \mathbf{M}_{q\theta} & \mathbf{M}_{qq}\end{bmatrix}^{-1}.
\end{aligned}
\tag{15}
$$

Hence, (13) can be decomposed as follows:

$$
\begin{aligned}
\ddot{\theta} &= -N_{\theta\theta}\left(\theta,\mathbf{q}\right)h_{\theta\theta}\left(\theta,\mathbf{q},\dot{\theta},\dot{\mathbf{q}}\right)\dot{\theta}\\
&- N_{\theta\theta}\left(\theta,\mathbf{q}\right)\mathbf{h}_{\theta q}\left(\theta,\mathbf{q},\dot{\theta},\dot{\mathbf{q}}\right)\dot{\mathbf{q}}\\
&- \mathbf{N}_{\theta q}\left(\theta,\mathbf{q}\right)\mathbf{h}_{q\theta}\left(\theta,\mathbf{q},\dot{\theta},\dot{\mathbf{q}}\right)\dot{\theta}\\
&- \mathbf{N}_{\theta q}\left(\theta,\mathbf{q}\right)\mathbf{h}_{qq}\left(\theta,\mathbf{q},\dot{\theta},\dot{\mathbf{q}}\right)\dot{\mathbf{q}}\\
&- \mathbf{N}_{\theta q}\left(\theta,\mathbf{q}\right)K_{qq}\mathbf{q} + N_{\theta\theta}\left(\theta,\mathbf{q}\right)\tau\\
&+ \left[N_{\theta\theta}\left(\theta,\mathbf{q}\right)\mathbf{g}_\theta + \mathbf{N}_{\theta q}\left(\theta,\mathbf{q}\right)\mathbf{g}_q\right]\mathbf{U},\\
\ddot{\mathbf{q}} &= -\mathbf{N}_{q\theta}\left(\theta,\mathbf{q}\right)h_{\theta\theta}\left(\theta,\mathbf{q},\dot{\theta},\dot{\mathbf{q}}\right)\dot{\theta}\\
&- \mathbf{N}_{q\theta}\left(\theta,\mathbf{q}\right)\mathbf{h}_{\theta q}\left(\theta,\mathbf{q},\dot{\theta},\dot{\mathbf{q}}\right)\dot{\mathbf{q}}\\
&- \mathbf{N}_{qq}\left(\theta,\mathbf{q}\right)\mathbf{h}_{q\theta}\left(\theta,\mathbf{q},\dot{\theta},\dot{\mathbf{q}}\right)\dot{\theta}\\
&- \mathbf{N}_{qq}\left(\theta,\mathbf{q}\right)\mathbf{h}_{qq}\left(\theta,\mathbf{q},\dot{\theta},\dot{\mathbf{q}}\right)\dot{\mathbf{q}} - \mathbf{N}_{qq}\left(\theta,\mathbf{q}\right)K_{qq}\mathbf{q}\\
&+ \mathbf{N}_{q\theta}\left(\theta,\mathbf{q}\right)\tau\\
&+ \left[\mathbf{N}_{q\theta}\left(\theta,\mathbf{q}\right)\mathbf{g}_\theta + \mathbf{N}_{qq}\left(\theta,\mathbf{q}\right)\mathbf{g}_q\right]\mathbf{U}.
\end{aligned}
\tag{16}
$$

Assuming that k_c is the smallest element of the stiffness matrix $\mathbf{K}$, then define new variable $\varepsilon = \sqrt{1/k_c}$. When k_c is big enough, $\varepsilon \to 0$. Then the new variables are defined as [7]

$$
\begin{aligned}
\boldsymbol{\xi} &= \frac{\mathbf{q}}{\varepsilon^2},\\
\widetilde{\mathbf{K}}_{qq} &= \varepsilon^2\mathbf{K}_{qq}.
\end{aligned}
\tag{17}
$$

Equation (17) is substituted into (16), the dynamics equation of the SFM can be represented in singular perturbation form as

$$
\begin{aligned}
\ddot{\theta} &= -N_{\theta\theta}\left(\theta,\varepsilon^2\boldsymbol{\xi}\right)h_{\theta\theta}\left(\theta,\varepsilon^2\boldsymbol{\xi},\dot{\theta},\varepsilon^2\dot{\boldsymbol{\xi}}\right)\dot{\theta}\\
&- \varepsilon^2 N_{\theta\theta}\left(\theta,\varepsilon^2\boldsymbol{\xi}\right)\mathbf{h}_{\theta q}\left(\theta,\varepsilon^2\boldsymbol{\xi},\dot{\theta},\varepsilon^2\dot{\boldsymbol{\xi}}\right)\dot{\boldsymbol{\xi}}\\
&- \mathbf{N}_{\theta q}\left(\theta,\varepsilon^2\boldsymbol{\xi}\right)\mathbf{h}_{q\theta}\left(\theta,\varepsilon^2\boldsymbol{\xi},\dot{\theta},\varepsilon^2\dot{\boldsymbol{\xi}}\right)\dot{\theta}\\
&- \varepsilon^2\mathbf{N}_{\theta q}\left(\theta,\varepsilon^2\boldsymbol{\xi}\right)\mathbf{h}_{qq}\left(\theta,\varepsilon^2\boldsymbol{\xi},\dot{\theta},\varepsilon^2\dot{\boldsymbol{\xi}}\right)\dot{\boldsymbol{\xi}}\\
&- \mathbf{N}_{\theta q}\left(\theta,\varepsilon^2\boldsymbol{\xi}\right)\widetilde{K}_{qq}\boldsymbol{\xi} + N_{\theta\theta}\left(\theta,\varepsilon^2\boldsymbol{\xi}\right)\tau\\
&+ \left[N_{\theta\theta}\left(\theta,\varepsilon^2\boldsymbol{\xi}\right)\mathbf{g}_\theta + \mathbf{N}_{\theta q}\left(\theta,\varepsilon^2\boldsymbol{\xi}\right)\mathbf{g}_q\right]\mathbf{U},\\
\varepsilon^2\ddot{\boldsymbol{\xi}} &= -\mathbf{N}_{q\theta}\left(\theta,\varepsilon^2\boldsymbol{\xi}\right)h_{\theta\theta}\left(\theta,\varepsilon^2\boldsymbol{\xi},\dot{\theta},\varepsilon^2\dot{\boldsymbol{\xi}}\right)\dot{\theta}\\
&- \varepsilon^2\mathbf{N}_{q\theta}\left(\theta,\varepsilon^2\boldsymbol{\xi}\right)\mathbf{h}_{\theta q}\left(\theta,\varepsilon^2\boldsymbol{\xi},\dot{\theta},\varepsilon^2\dot{\boldsymbol{\xi}}\right)\dot{\boldsymbol{\xi}}\\
&- \mathbf{N}_{qq}\left(\theta,\varepsilon^2\boldsymbol{\xi}\right)\mathbf{h}_{q\theta}\left(\theta,\varepsilon^2\boldsymbol{\xi},\dot{\theta},\varepsilon^2\dot{\boldsymbol{\xi}}\right)\dot{\theta}\\
&- \varepsilon^2\mathbf{N}_{qq}\left(\theta,\varepsilon^2\boldsymbol{\xi}\right)\mathbf{h}_{qq}\left(\theta,\varepsilon^2\boldsymbol{\xi},\dot{\theta},\varepsilon^2\dot{\boldsymbol{\xi}}\right)\dot{\boldsymbol{\xi}}\\
&- \mathbf{N}_{qq}\left(\theta,\varepsilon^2\boldsymbol{\xi}\right)\widetilde{K}_{qq}\boldsymbol{\xi} + \mathbf{N}_{q\theta}\left(\theta,\varepsilon^2\boldsymbol{\xi}\right)\tau\\
&+ \left[\mathbf{N}_{q\theta}\left(\theta,\varepsilon^2\boldsymbol{\xi}\right)\mathbf{g}_\theta + \mathbf{N}_{qq}\left(\theta,\varepsilon^2\boldsymbol{\xi}\right)\mathbf{g}_q\right]\mathbf{U}.
\end{aligned}
\tag{18}
$$

$$
\begin{aligned}
\ddot{\theta} &= -N_{\theta\theta}\left(\theta,\varepsilon^2\boldsymbol{\xi}\right)h_{\theta\theta}\left(\theta,\varepsilon^2\boldsymbol{\xi},\dot{\theta},\varepsilon^2\dot{\boldsymbol{\xi}}\right)\dot{\theta}\\
&- \varepsilon^2 N_{\theta\theta}\left(\theta,\varepsilon^2\boldsymbol{\xi}\right)\mathbf{h}_{\theta q}\left(\theta,\varepsilon^2\boldsymbol{\xi},\dot{\theta},\varepsilon^2\dot{\boldsymbol{\xi}}\right)\dot{\boldsymbol{\xi}}\\
&- \mathbf{N}_{\theta q}\left(\theta,\varepsilon^2\boldsymbol{\xi}\right)\mathbf{h}_{q\theta}\left(\theta,\varepsilon^2\boldsymbol{\xi},\dot{\theta},\varepsilon^2\dot{\boldsymbol{\xi}}\right)\dot{\theta}\\
&- \varepsilon^2\mathbf{N}_{\theta q}\left(\theta,\varepsilon^2\boldsymbol{\xi}\right)\mathbf{h}_{qq}\left(\theta,\varepsilon^2\boldsymbol{\xi},\dot{\theta},\varepsilon^2\dot{\boldsymbol{\xi}}\right)\dot{\boldsymbol{\xi}}\\
&- \mathbf{N}_{\theta q}\left(\theta,\varepsilon^2\boldsymbol{\xi}\right)\widetilde{K}_{qq}\boldsymbol{\xi} + N_{\theta\theta}\left(\theta,\varepsilon^2\boldsymbol{\xi}\right)\tau\\
&+ \left[N_{\theta\theta}\left(\theta,\varepsilon^2\boldsymbol{\xi}\right)\mathbf{g}_\theta + \mathbf{N}_{\theta q}\left(\theta,\varepsilon^2\boldsymbol{\xi}\right)\mathbf{g}_q\right]\mathbf{U},\\
\varepsilon^2\ddot{\boldsymbol{\xi}} &= -\mathbf{N}_{q\theta}\left(\theta,\varepsilon^2\boldsymbol{\xi}\right)h_{\theta\theta}\left(\theta,\varepsilon^2\boldsymbol{\xi},\dot{\theta},\varepsilon^2\dot{\boldsymbol{\xi}}\right)\dot{\theta}\\
&- \varepsilon^2\mathbf{N}_{q\theta}\left(\theta,\varepsilon^2\boldsymbol{\xi}\right)\mathbf{h}_{\theta q}\left(\theta,\varepsilon^2\boldsymbol{\xi},\dot{\theta},\varepsilon^2\dot{\boldsymbol{\xi}}\right)\dot{\boldsymbol{\xi}}\\
&- \mathbf{N}_{qq}\left(\theta,\varepsilon^2\boldsymbol{\xi}\right)\mathbf{h}_{q\theta}\left(\theta,\varepsilon^2\boldsymbol{\xi},\dot{\theta},\varepsilon^2\dot{\boldsymbol{\xi}}\right)\dot{\theta}\\
&- \varepsilon^2\mathbf{N}_{qq}\left(\theta,\varepsilon^2\boldsymbol{\xi}\right)\mathbf{h}_{qq}\left(\theta,\varepsilon^2\boldsymbol{\xi},\dot{\theta},\varepsilon^2\dot{\boldsymbol{\xi}}\right)\dot{\boldsymbol{\xi}}\\
&- \mathbf{N}_{qq}\left(\theta,\varepsilon^2\boldsymbol{\xi}\right)\widetilde{K}_{qq}\boldsymbol{\xi} + \mathbf{N}_{q\theta}\left(\theta,\varepsilon^2\boldsymbol{\xi}\right)\tau\\
&+ \left[\mathbf{N}_{q\theta}\left(\theta,\varepsilon^2\boldsymbol{\xi}\right)\mathbf{g}_\theta + \mathbf{N}_{qq}\left(\theta,\varepsilon^2\boldsymbol{\xi}\right)\mathbf{g}_q\right]\mathbf{U}.
\end{aligned}
\tag{19}
$$

3.1. Slow Subsystem. To derive the boundary layer correction, ε is set to zero and the model of the rigid manipulator is expressed as

$$\begin{aligned}\ddot{\theta} = & -N_{\theta\theta}(\theta,0)\, h_{\theta\theta}\left(\theta,0,\dot{\theta},0\right)\dot{\theta} \\ & - \mathbf{N}_{\theta q}(\theta,0)\, \mathbf{h}_{q\theta}\left(\theta,0,\dot{\theta},0\right)\dot{\theta} - \mathbf{N}_{\theta q}(\theta,0)\, \widetilde{K}_{qq}\boldsymbol{\xi} \\ & + N_{\theta\theta}(\theta,0)\, \tau_s \\ & + \left[N_{\theta\theta}(\theta,0)\, \mathbf{g}_\theta + \mathbf{N}_{\theta q}(\theta,0)\, \mathbf{g}_q\right]\mathbf{U}_s,\end{aligned} \tag{20}$$

$$\begin{aligned}0 = & -\mathbf{N}_{q\theta}(\theta,0)\, h_{\theta\theta}\left(\theta,0,\dot{\theta},0\right)\dot{\theta} \\ & - \mathbf{N}_{qq}(\theta,0)\, \mathbf{h}_{q\theta}\left(\theta,0,\dot{\theta},0\right)\dot{\theta} - \mathbf{N}_{qq}(\theta,0)\, \widetilde{K}_{qq}\boldsymbol{\xi} \\ & + \mathbf{N}_{q\theta}(\theta,0)\, \tau_s \\ & + \left[\mathbf{N}_{q\theta}(\theta,0)\, \mathbf{g}_\theta + \mathbf{N}_{qq}(\theta,0)\, \mathbf{g}_q\right]\mathbf{U}_s.\end{aligned} \tag{21}$$

Combining (15), (20), and (21), the slow subsystem is given by

$$\ddot{\theta} = \left[\overline{M}_{\theta\theta}\right]^{-1}\left\{-\overline{h}_{\theta\theta}\dot{\theta} + \tau_s + \mathbf{g}_\theta \mathbf{U}_s\right\}, \tag{22}$$

where τ_s is the control torque of slow time scale subsystem and $\mathbf{U}_s$ is the control voltage of slow time scale subsystem.

3.2. Fast Subsystem. To derive the fast subsystem, introduce a fast time scale $\gamma = t/\varepsilon$ and define boundary layer variables as [21]

$$\begin{aligned}\boldsymbol{\eta}_1 &= \boldsymbol{\xi} - \overline{\boldsymbol{\xi}}, \\ \boldsymbol{\eta}_2 &= \varepsilon\dot{\boldsymbol{\xi}}.\end{aligned} \tag{23}$$

Then (19) is written as

$$\frac{d\boldsymbol{\eta}_1}{d\gamma} = \boldsymbol{\eta}_2, \tag{24a}$$

$$\begin{aligned}\frac{d\boldsymbol{\eta}_2}{d\gamma} = & -\mathbf{N}_{q\theta}\left(\theta,\varepsilon^2\left(\boldsymbol{\eta}_1+\overline{\boldsymbol{\xi}}\right)\right) \\ & \cdot h_{\theta\theta}\left(\theta,\varepsilon^2\left(\boldsymbol{\eta}_1+\overline{\boldsymbol{\xi}}\right),\dot{\theta},\varepsilon\boldsymbol{\eta}_2\right)\dot{\theta} \\ & - \varepsilon\mathbf{N}_{q\theta}\left(\theta,\varepsilon^2\left(\boldsymbol{\eta}_1+\overline{\boldsymbol{\xi}}\right)\right) \\ & \cdot \mathbf{h}_{\theta q}\left(\theta,\varepsilon^2\left(\boldsymbol{\eta}_1+\overline{\boldsymbol{\xi}}\right),\dot{\theta},\varepsilon\boldsymbol{\eta}_2\right)\boldsymbol{\eta}_2 \\ & - \mathbf{N}_{qq}\left(\theta,\varepsilon^2\left(\boldsymbol{\eta}_1+\overline{\boldsymbol{\xi}}\right)\right)\mathbf{h}_{q\theta}\left(\theta,\varepsilon^2\left(\boldsymbol{\eta}_1+\overline{\boldsymbol{\xi}}\right),\dot{\theta},\varepsilon\boldsymbol{\eta}_2\right) \\ & \cdot \dot{\theta} - \varepsilon\mathbf{N}_{qq}\left(\theta,\varepsilon^2\left(\boldsymbol{\eta}_1+\overline{\boldsymbol{\xi}}\right)\right) \\ & \cdot \mathbf{h}_{qq}\left(\theta,\varepsilon^2\left(\boldsymbol{\eta}_1+\overline{\boldsymbol{\xi}}\right),\dot{\theta},\varepsilon\boldsymbol{\eta}_2\right)\boldsymbol{\eta}_2 \\ & - \mathbf{N}_{qq}\left(\theta,\varepsilon^2\left(\boldsymbol{\eta}_1+\overline{\boldsymbol{\xi}}\right)\right)\widetilde{K}_{qq}\left(\boldsymbol{\eta}_1+\overline{\boldsymbol{\xi}}\right) \\ & + \mathbf{N}_{q\theta}\left(\theta,\varepsilon^2\left(\boldsymbol{\eta}_1+\overline{\boldsymbol{\xi}}\right)\right)\tau \\ & + \left[\mathbf{N}_{q\theta}\left(\theta,\varepsilon^2\left(\boldsymbol{\eta}_1+\overline{\boldsymbol{\xi}}\right)\right)\mathbf{g}_\theta \right. \\ & \left. + \mathbf{N}_{qq}\left(\theta,\varepsilon^2\left(\boldsymbol{\eta}_1+\overline{\boldsymbol{\xi}}\right)\right)\mathbf{g}_q\right]\mathbf{U}.\end{aligned} \tag{24b}$$

Because the slow time scale and fast time scale are independent of each other, near boundary layer region $\varepsilon \to 0$ and the slow varying component can be regarded as constant ($d\boldsymbol{\xi}/d\gamma = \varepsilon\boldsymbol{\xi} = 0$). Assuming that $\varepsilon = 0$ and (21) are substituted into (24a) and (24b), the fast subsystem is expressed as

$$\frac{d\boldsymbol{\eta}_1}{d\gamma} = \boldsymbol{\eta}_2, \tag{25a}$$

$$\frac{d\boldsymbol{\eta}_2}{d\gamma} = -\overline{\mathbf{N}}_{qq}\widetilde{\mathbf{K}}_{qq}\boldsymbol{\eta}_1 + \overline{\mathbf{N}}_{q\theta}\left(\tau_f + \mathbf{g}_\theta \mathbf{U}_f\right) + \overline{\mathbf{N}}_{qq}\mathbf{g}_q\mathbf{U}_f, \tag{25b}$$

where τ_f is the control torque of fast time scale subsystem and $\mathbf{U}_f$ is the control voltage of fast time scale subsystem.

4. Design of the Composite Controller

The control objective is to track the desired trajectory and suppress the vibration of the SFM. As shown in Figure 3, the control torque τ_s and control voltage $\mathbf{U}_s$ for trajectory tracking are got by slow subsystem controller and the control torque τ_f and control voltage $\mathbf{U}_f$ for vibration suppression are got by fast subsystem controller. The total inputs of controller are gained as $\tau = \tau_s + \tau_f$ and $\mathbf{U} = \mathbf{U}_s + \mathbf{U}_f$. In this section, the slow subsystem controller is designed by fuzzy sliding mode control method, and the linear quadratic regulator (LQR) optimal control method is used to design fast subsystem controller.

4.1. Slow Subsystem Controller Design. Assuming the desired trajectory as $\theta_d(t)$, the trajectory tracking error $e(t)$ and speed tracking error $\dot{e}(t)$ can be written as [22]

$$\begin{aligned}e(t) &= \theta_d(t) - \theta(t), \\ \dot{e}(t) &= \dot{\theta}_d(t) - \dot{\theta}(t).\end{aligned} \tag{26}$$

Define a sliding surface s as

$$s = \dot{e}(t) + \lambda e(t), \tag{27}$$

where λ is positive proportionality coefficient.

Obviously, if the slow subsystem states stay on the sliding mode surface, it ensures that $\theta(t) \to \theta_d(t)$ and $\dot{\theta}(t) \to \dot{\theta}_d(t)$ and can realize the trajectory tracking control. The exponential reaching law function is shown as

$$\dot{s} = -\psi\,\mathrm{sgn}(s) - \delta s, \quad \psi > 0,\ \delta > 0. \tag{28}$$

Taking the derivative of the sliding surface $\dot{s}$ and (22) which are substituted into it, then (29) is obtained as

$$\begin{aligned}\dot{s} = \ddot{e}(t) + \lambda\dot{e}(t) &= \ddot{\theta}_d(t) - \ddot{\theta}(t) + \lambda\dot{e}(t) \\ &= \ddot{\theta}_d(t) - \left[\overline{M}_{\theta\theta}\right]^{-1}\left\{\tau_s + \mathbf{g}_\theta\mathbf{U}_s - \overline{h}_{\theta\theta}\dot{\theta}\right\} + \lambda\dot{e}(t).\end{aligned} \tag{29}$$

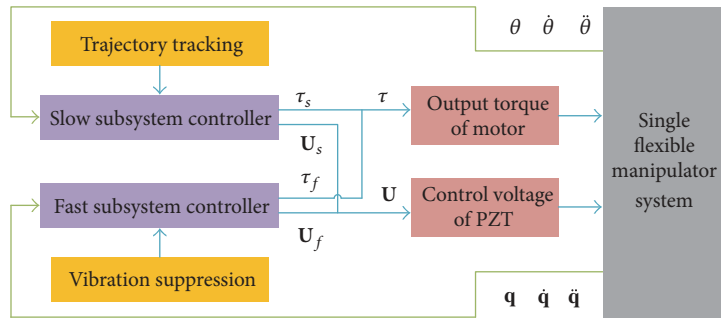

Figure 3: Structure diagram of the composite controller.

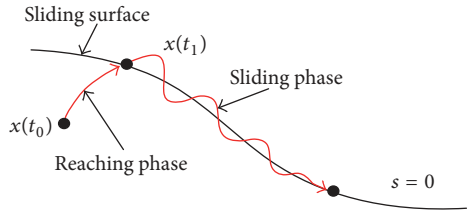

Figure 4: Generic sliding surface.

Equation (28) is substituted into (29); the control law is expressed as

$$\tau_s = \overline{M}_{\theta\theta}\left[\ddot{\theta}_d(t) + \lambda\left(\dot{\theta}_d(t) - \dot{\theta}(t)\right) + \psi\,\mathrm{sgn}(s) + \delta s\right] - \mathbf{g}_\theta \mathbf{U}_s + \overline{h}_{\theta\theta}\dot{\theta}. \tag{30}$$

A sliding mode controller has two phases; the first is called the reaching phase. During this phase the controller is guiding the system state onto the sliding surface. The second phase is called the sliding phase, during which the system state "slides" along the sliding surface [23]. Figure 4 shows the generic sliding surface. Therefore, the chattering with high frequency in sliding mode control systems is a barrier for the application to the practice engineering problems. It is known that, based on the fuzzy sets, fuzzy language variables, and fuzzy logic inference, as a popular nonlinear control theory, fuzzy control has been widely used in industrial control systems. Using fuzzy control method, the switching variable of sliding mode control can be adjusted adaptively according to expertise, and it can effectively weaken the chattering phenomenon and strengthen the robustness of system.

The adaptive fuzzy sliding mode controller is illustrated in Figure 5. In the sliding mode controller, the switching variable ψ is selected as a time-varying value which is denoted as $\mathbf{\Psi}$ and realized by fuzzy controller. Based on the two-dimensional fuzzy controller, the sliding surface s and its derivative $\dot{s}$ are selected as the inputs of fuzzy controller, and the switching variable ψ is selected as the output of fuzzy controller. Linguistic variables correspond to seven different linguistic terms {NB, NM, NS, ZO, PS, PM, PB}, abbreviation of "Negative Big," "Negative Middle," "Negative Small," "Zero," "Positive Small," "Positive Middle," "Positive Big," respectively. In addition, one should define the relevant proportional factors from the experimental test data to linguistic levels. The linguistic variables S, DS, and $\mathbf{\Psi}$ represent sliding surface s, derivative of the sliding surface $\dot{s}$, and switching variable ψ in the fuzzy set [24]. The universes of discourses of S, DS, and $\mathbf{\Psi}$ are from −1 to 1, −1 to 1, and 0 to 1, respectively. Then [24]

$$S = k_1 s, \tag{31}$$

where $k_1 = 1/|s_{\max}|$ and $s_{\max}$ is the maximum value of the sliding surface s.

$$DS = k_2 \dot{s}, \tag{32}$$

where $k_2 = 1/|\dot{s}_{\max}|$ and $\dot{s}_{\max}$ is the maximum value of derivative of the sliding surface $\dot{s}$.

$$\psi = k_3 \mathbf{\Psi}, \tag{33}$$

where $k_3 = \psi_{\max}/1$ and $\psi_{\max}$ is the maximum value allowed for switching variable ψ.

$s_{\max}$, $\dot{s}_{\max}$, and $\psi_{\max}$ are chosen from numerical simulations.

Seven linguistic levels (NB, NM, NS, ZO, PS, PM, and PB) are used to represent the input domain and output domain with their membership values lying between 0 and 1 [24]. The basic triangular and Z forms are chosen for the input and output membership functions [25, 26]. The membership functions are employed to convert these input and output variables into linguistic control variables (NB, NM, NS, ZO, PS, PM, and PB) and the membership functions are shown in Figure 6.

Table 1 shows the generated fuzzy inference rules of fuzzy controller [25], and the surface of the fuzzy rules is shown in Figure 7. The fuzzy inference rules are designed based on the changes of the sliding surface s and its derivative which are obtained by simulations.

4.2. Fast Subsystem Controller Design. Define boundary layer variables as $\boldsymbol{\eta} = [\boldsymbol{\eta}_1, \boldsymbol{\eta}_2]^T$; (25a) and (25b) are rewritten as

$$\dot{\boldsymbol{\eta}} = \mathbf{A}_f \boldsymbol{\eta} + \mathbf{B}_f \mathbf{u}_f, \tag{34}$$

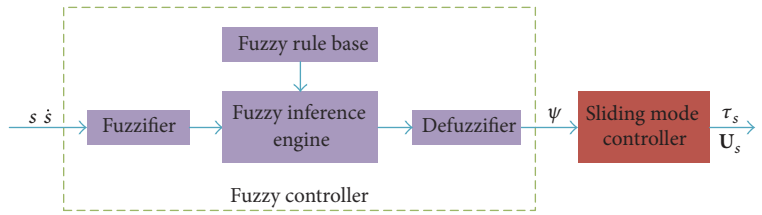

Figure 5: Adaptive fuzzy sliding mode controller.

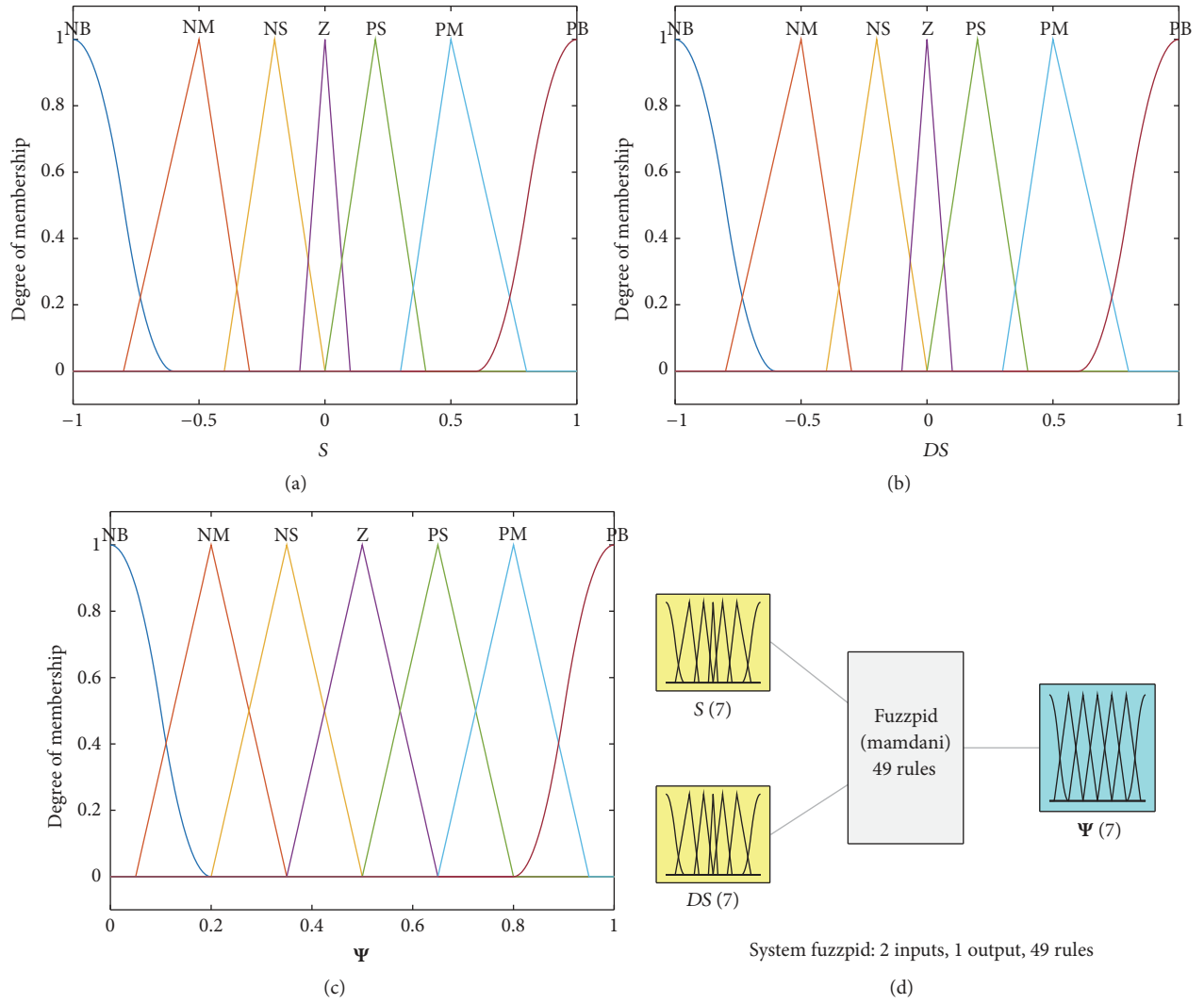

Figure 6: Membership functions of fuzzy controller ((a) linguistic variable S; (b) linguistic variable DS; (c) linguistic variable $\boldsymbol{\Psi}$; (d) schematic of fuzzy inference).

where

$$\mathbf{A}_f = \begin{bmatrix} 0 & \mathbf{I} \\ -\overline{\mathbf{N}}_{qq}\widetilde{\mathbf{K}}_{qq} & 0 \end{bmatrix},$$
$$\mathbf{B}_f = \begin{bmatrix} 0 & 0 \\ \overline{\mathbf{N}}_{q\theta} & \overline{\mathbf{N}}_{q\theta}\mathbf{g}_\theta + \overline{\mathbf{N}}_{qq}\mathbf{g}_q \end{bmatrix}, \quad (35)$$
$$\mathbf{u}_f = \left[\tau_f, \mathbf{U}_f\right]^T.$$

It can be seen that the fast subsystem, as described by (34), is in a linear feedback form, for which the fast subsystem controller is designed using LQR method. The optimal control block diagram of the fast subsystem is shown in Figure 8.

To damp out the flexible vibration and decrease the control effort, the quadratic objective function is chosen as

$$J = \frac{1}{2}\int_0^\infty \left(\boldsymbol{\eta}^T\mathbf{Q}\boldsymbol{\eta} + \mathbf{u}_f{}^T\mathbf{R}\mathbf{u}_f\right)dt, \quad (36)$$

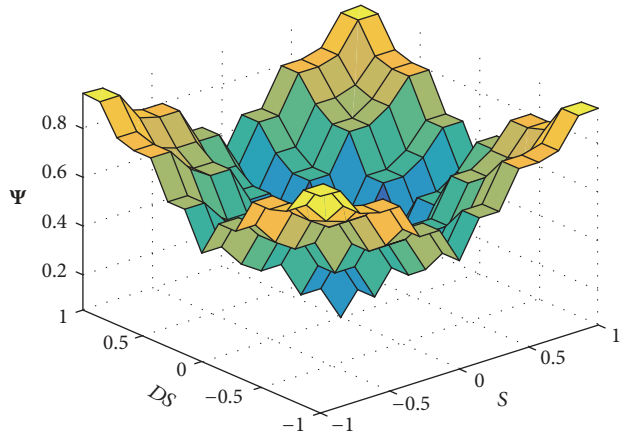

Figure 7: Surface of the fuzzy rules.

Table 1: Fuzzy inference rules of fuzzy controller.

Ψ				S			
DS	NB	NM	NS	ZO	PS	PM	PB
NB	PB	PM	PS	ZO	PS	PM	PB
NM	PM	PS	ZO	NS	ZO	PS	PM
NS	PS	ZO	NS	NM	NS	ZO	PS
ZO	ZO	NS	NM	NB	NM	NS	ZO
PS	PS	ZO	NS	NM	NS	ZO	PS
PM	PM	PS	ZO	NS	ZO	PS	PM
PM	PB	PM	PS	ZO	PS	PM	PB

where $\mathbf{Q}$ and $\mathbf{R}$ are weighting matrix for state variables and control effort, respectively, and $\mathbf{u}_f$ represents the input or control variable of the fast subsystem system. Then, the optimum control input for fast subsystem is determined as [21]

$$\mathbf{u}_f = -\mathbf{K}_f\boldsymbol{\eta} = -\mathbf{R}^{-1}{\mathbf{B}_f}^T\mathbf{P}\boldsymbol{\eta}, \tag{37}$$

where $\mathbf{K}_f$ is the feedback gain matrix and $\mathbf{P}$ is the solutions of the Riccati equation as follows:

$$\mathbf{P}\mathbf{A}_f + {\mathbf{A}_f}^T\mathbf{P} - \mathbf{P}\mathbf{B}_f\mathbf{R}^{-1}{\mathbf{B}_f}^T\mathbf{P} + \mathbf{Q} = 0. \tag{38}$$

5. Optimal Placement and Composite Control of the SFM

To verify the composite control strategy on the trajectory tracking and vibration suppression of the SFM, numerical simulations are conducted in this section. Owing to the lower order modes play leading role in the vibration of the SFM, only the first two order modes are considered, and the active control simulations are performed using the independent mode space control method. The structural parameters of the SFM and actuators are shown in Tables 2 and 3, respectively.

5.1. Optimal Placement of Actuators. The three-dimensional model of the SFM with surface bonded actuators is established by ANSYS Workbench software, and it is shown as Figure 9. Then, the position of the piezoelectric actuator is set as input parameter, and the first-order natural frequency and second-order natural frequency are set as output parameters. Based on the response surface method, the changing trends of natural frequencies along with the position of piezoelectric actuator are shown as Figure 10. From Figure 10(a), the maximum value of the first-order natural frequency is got when the piezoelectric actuator is bonded in the root of the SFM. The maximum value of the second-order natural frequency is in root, and the second maximum value is in the position of $x = 0.255$ m, as shown in Figure 10(b). Hence, the first pair of piezoelectric actuators should be bonded in the root of the SFM and the second pair of piezoelectric actuators should be bonded in the position of $x = 0.255$ mm. That is, $a_{11} = 0$ m and $a_{12} = 0.04$ m; $a_{21} = 0.255$ m and $a_{22} = 0.295$ m.

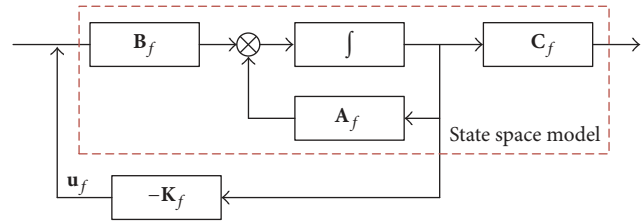

Figure 8: Optimal control block diagram of the fast subsystem.

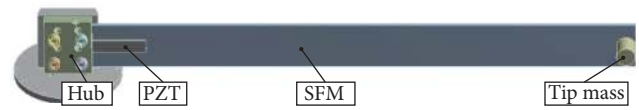

Figure 9: Three-dimensional model of the SFM with surface bonded actuators.

Table 2: Structural parameters of SFM.

Parameter	Value	Unit
Length L_b	0.400	m
Width b_b	0.035	m
Thickness t_b	0.0027	m
Density ρ_b	2.03×10^3	kg/m^3
Elastic modulus E_b	25.24	GPa
Rotational inertia J_h	2.5×10^{-4}	kg·m^2
Hub radius r	0.0175	m
Tip mass m_L	0.03	kg

Table 3: Structural parameters of actuators.

Parameter	Value	Unit
Length L_p	0.04	m
Width b_p	0.01	m
Thickness t_p	0.0008	m
Density ρ_p	7.65×10^3	kg/m^3
Elastic modulus E_p	57.3	GPa

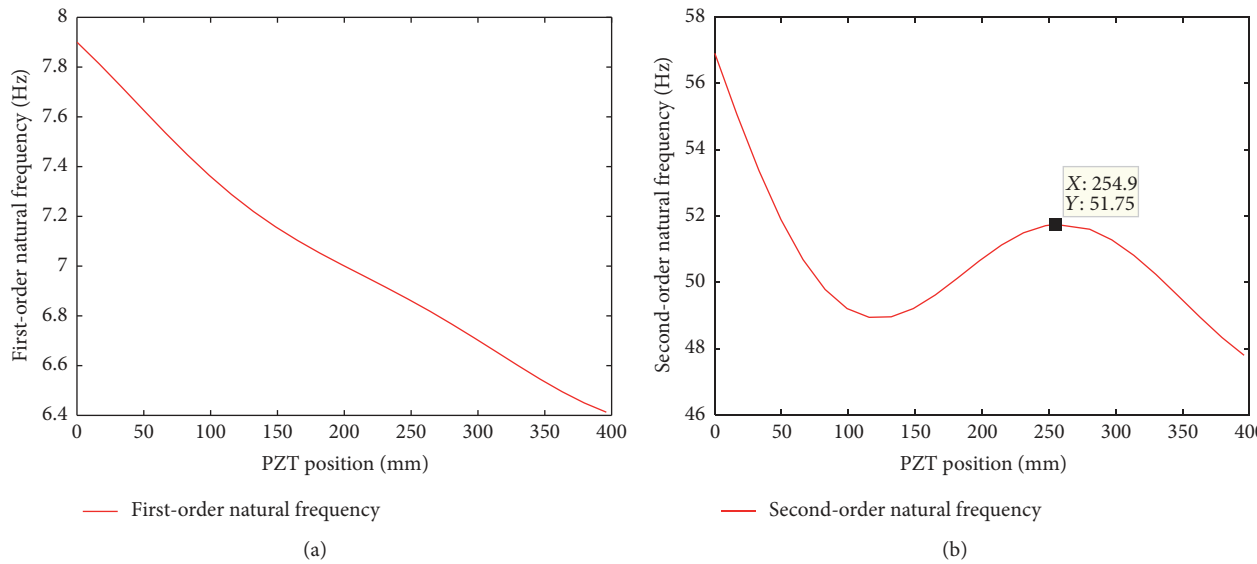

(a) (b)

Figure 10: Changing trends of natural frequencies along with the position of piezoelectric actuator ((a) first-order natural frequency; (b) second-order natural frequency).

5.2. Numerical Simulations. The angular displacement trajectory of the SFM is shown as

$$\theta_d(t) = \left[6\left(\frac{t}{t_e}\right)^5 - 15\left(\frac{t}{t_e}\right)^4 + 10\left(\frac{t}{t_e}\right)^3\right](\theta_e - \theta_0) + \theta_0. \quad (39)$$

The control parameters are chosen as follows.

(1) Adaptive Fuzzy Sliding Mode Controller. $\lambda = 50$, $\delta = 0.1$, $k_1 = 5$, $k_2 = 0.025$, $k_3 = 3$, and ψ is obtained by fuzzy controller.

(2) LQR Controller

$$\mathbf{Q} = \begin{bmatrix} 350000 & 0 & 0 & 0 \\ 0 & 10000 & 0 & 0 \\ 0 & 0 & 1000 & 0 \\ 0 & 0 & 0 & 100 \end{bmatrix}, \quad \mathbf{R} = \begin{bmatrix} 2 & 0 \\ 0 & 3 \end{bmatrix}. \quad (40)$$

The simulation curves of composite control for trajectory tracking and vibration suppression of the SFM are shown in Figure 11. Figure 11(a) shows the relation curve of the switching variable ψ with time, which is adjusted by fuzzy controller. Figures 11(b) and 11(c) show the output control of the speed reducer which is driven by a motor and the control voltage of actuators, respectively. Figure 11(d) shows the tip angle of the SFM, and it demonstrates that the composite controller successfully implements the trajectory tracking and vibration suppression of the SFM. Figures 11(e) and 11(f) show the first-order modal coordinate and second-order modal coordinate, respectively. It is obtained that the first-order modal coordinate is much larger than the second-order modal coordinate and illustrates that the lower order modes play leading role in the vibration of the SFM. The tip deflection of the SFM in a time-domain is obtained by the modal coordinates and shown in Figure 11(g). Meanwhile, it is evident from Figure 11(g) that the composite controller can successfully suppress the simultaneous elastic vibration in movement of the SFM. Figure 11(h) shows the structural strain history along the length of SFM for the first 3 s of the manipulator motion. It can be observed that the highest strain experienced occurs in the root of the SFM and the strain is reduced gradually in the control of composite controller.

5.3. Control Experiments. In order to better demonstrate the effectiveness of the composite controller, the experiments on composite control of the SFM are constructed. The overall experimental setup and the flowchart of composite control experiments are depicted in Figures 12 and 13, respectively.

The comparison between the simulated and experimental results of the SFM is shown in Figure 14. It can be seen that the results of the experimental results are in good agreement with the simulation result in Figure 11. Figure 14(d) shows the tip angle of the SFM, and it demonstrates that the composite controller successfully achieved the trajectory tracking of the SFM. Meanwhile, the elastic vibration in movement of the SFM is suppressed successfully by the composite controller and shown in Figure 14(e). Figure 14(f) shows that the strain trends of the SFM are got by strain gauges which are bonded below the PZTs, respectively. In addition, it should be noted that the results exhibit a certain error between the simulated and experimental results, and this is mainly caused by the difference between experiment system and dynamic model, such as viscous damping, air resistance, the machining precision of structure, and the precision of sensors.

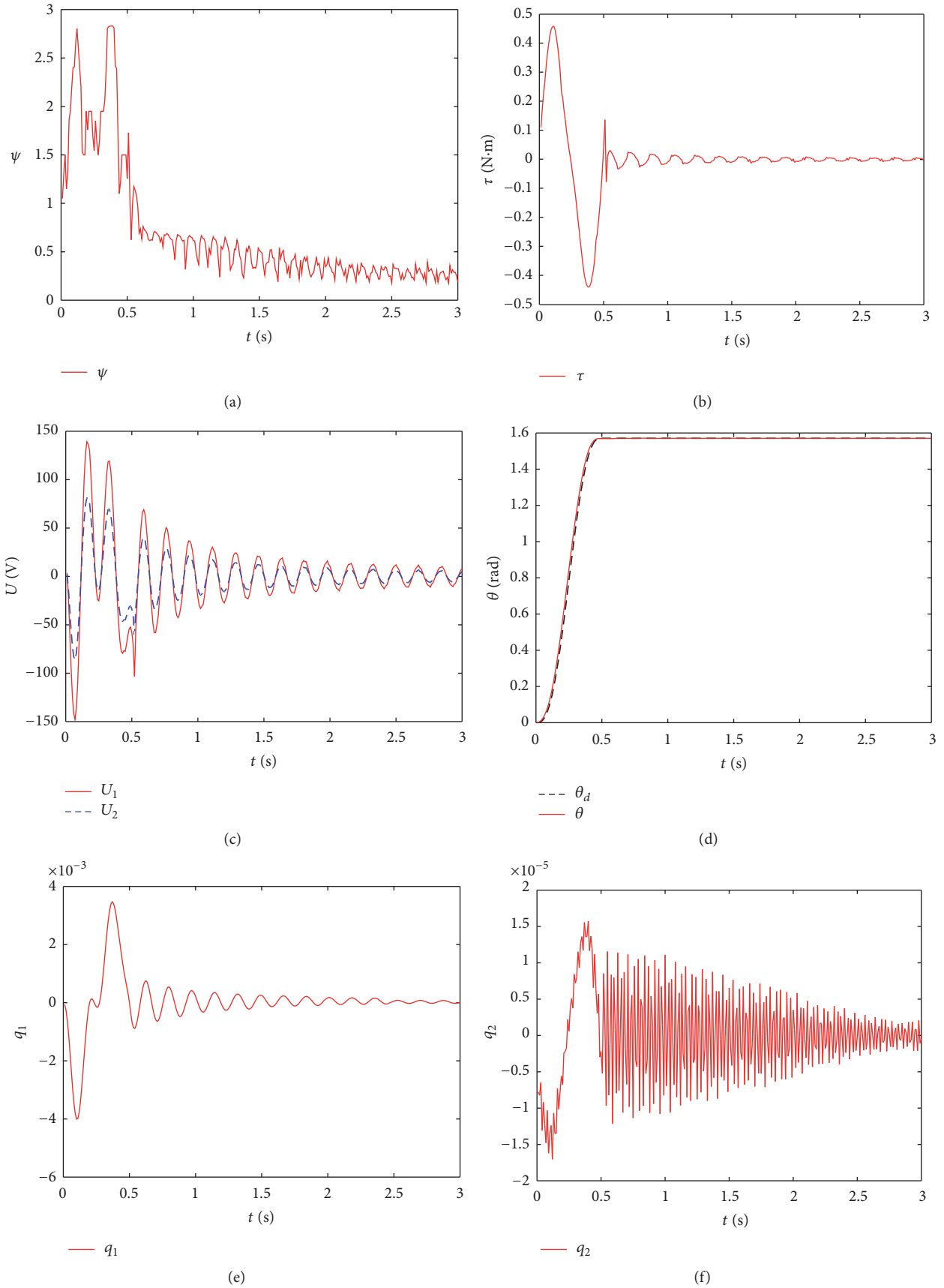

Figure 11: Continued.

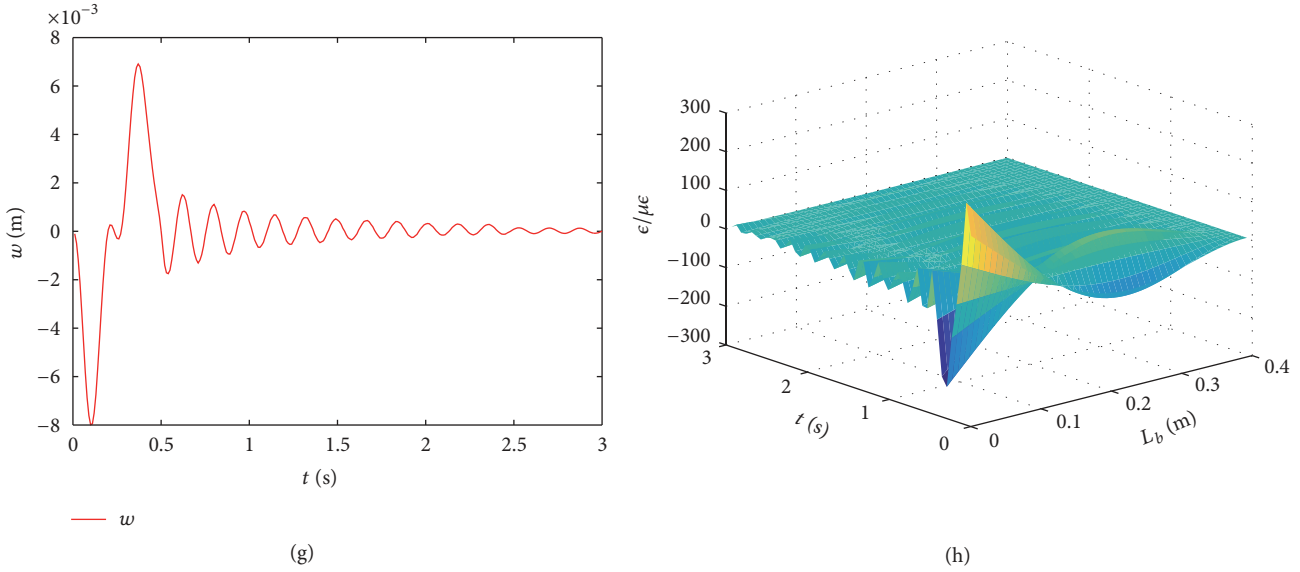

Figure 11: Simulation curves of composite control for trajectory tracking and vibration suppression of the SFM ((a) time-varying control variable; (b) control torque; (c) control voltage; (d) tip angle; (e) first-order modal coordinate; (f) second-order modal coordinate; (g) tip deflection; (h) strain time history).

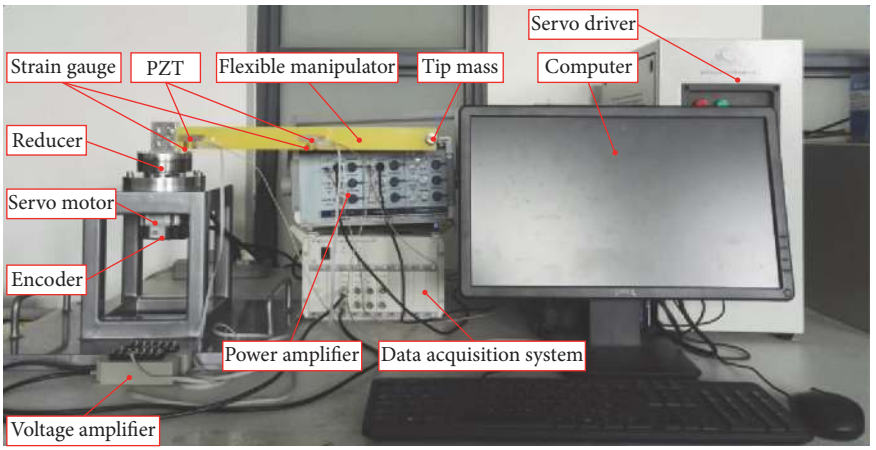

Figure 12: Photograph of the experimental apparatus.

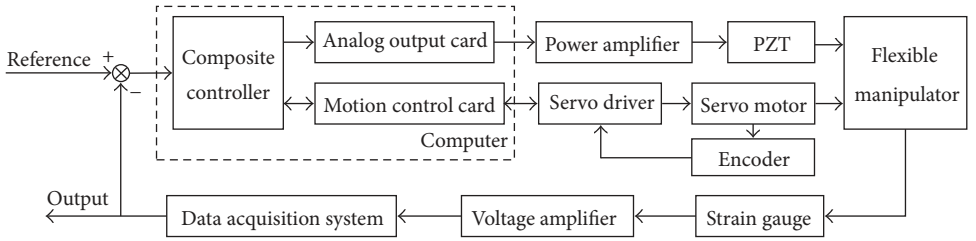

Figure 13: Flowchart of the composite control experiments.

6. Conclusions

This paper mainly discusses the modelling and composite control of the SFM with piezoelectric actuators. The dynamic model of the SFM with surface bonded actuators is described by means of the assumed mode method, piezoelectric coupling model, and Hamilton's principle. Based on the singular perturbation method, the coupled dynamic equation is decomposed into slow (rigid) and fast (flexible) subsystems. Then, the composite controller for the slow

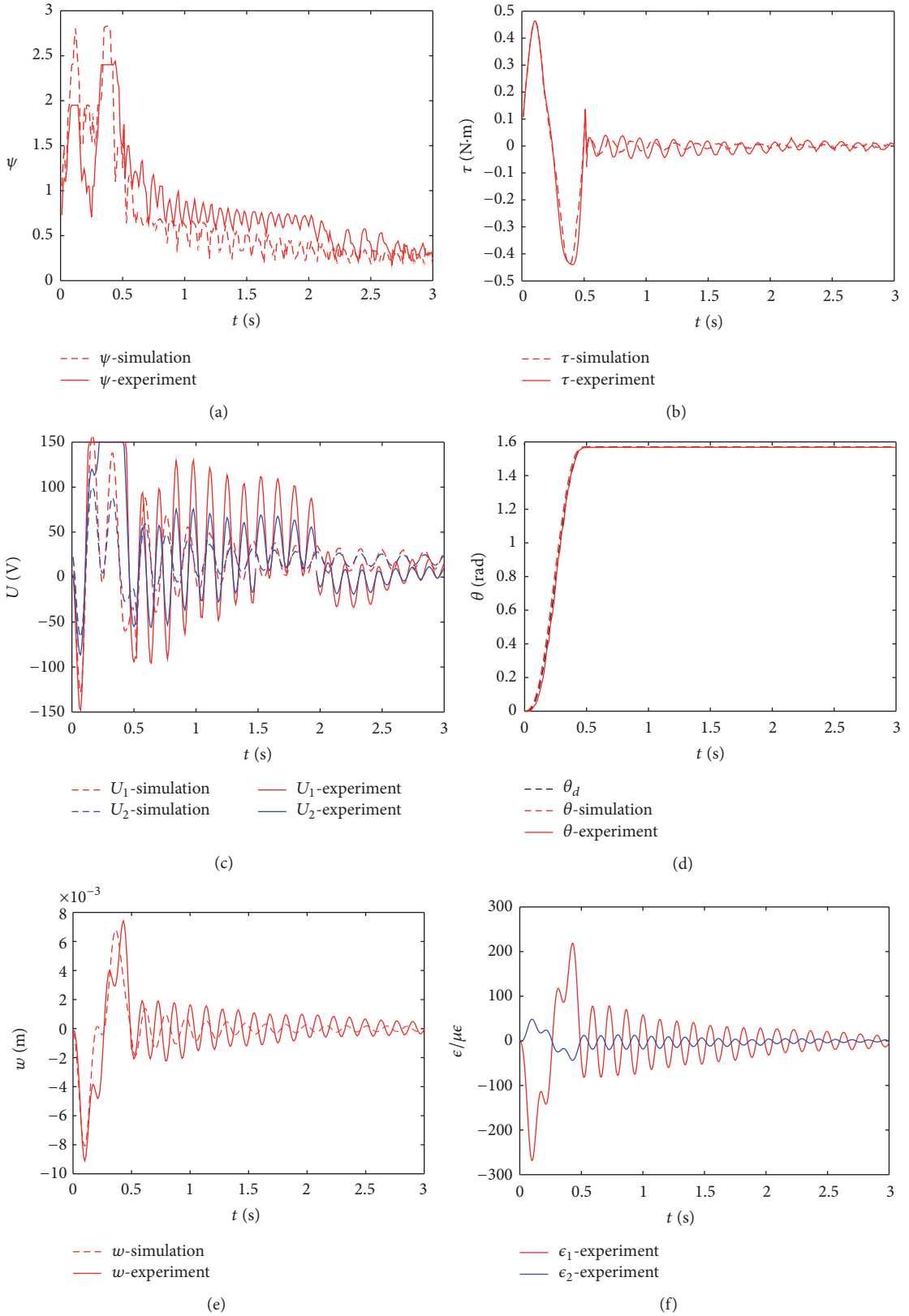

FIGURE 14: Comparison between the simulated and experimental results of the SFM ((a) time-varying control variable; (b) control torque; (c) control voltage; (d) tip angle; (e) tip deflection; (f) strain trend).

subsystem and fast subsystem is achieved using the fuzzy sliding mode control and LQR technique. Furthermore, the optimal placement of actuators is determined by the index of natural frequencies of SFM.

By the analysis of numerical simulation, the optimal placement of actuators is feasible based on the maximal natural frequency. Meanwhile, the composite controller presented in this paper can not only realize the trajectory tracking of the SFM and can successfully suppress the simultaneous elastic vibration in movement of the SFM, and the closed-loop stability of the SFM is achieved. In addition, the structural strain history along the length of SFM demonstrates that the highest strain experienced occurs in the root of the SFM in the early stage and the strain is reduced gradually in the control of composite controller. Finally, the experiments demonstrate that the control effect of the composite controller reaches the expectation and the experiment results are consistent with simulation results, which further demonstrated the feasibility of the proposed composite control method.

Competing Interests

The authors declare that there are no competing interests regarding the publication of this paper.

Acknowledgments

This research work was partially supported by the National Natural Science Foundation of China (no. 51305444 and no. 51307172), the Scientific and Technological Projects of Jiangsu Province (BY2014028-06), the Six Talent Peaks Project in Jiangsu Province (ZBZZ-041), the Postgraduate Cultivation and Innovation Project of Jiangsu Province (KYLX16_0523), and the Project Funded by the Priority Academic Program Development of Jiangsu Higher Education Institutions (PAPD).

References

[1] Y. F. Liu, W. Li, X. F. Yang, Y. Q. Wang, M. B. Fan, and G. Ye, "Coupled dynamic model and vibration responses characteristic of a motor-driven flexible manipulator system," *Mechanical Sciences*, vol. 6, no. 2, pp. 235–244, 2015.

[2] J. Y. Ju, W. Li, Y. Q. Wang, M. Fan, X. Yang, and Y. Liu, "Vibration observation for a translational flexible-link manipulator based on improved Luenberger observer," *Journal of Vibroengineering*, vol. 18, no. 1, pp. 238–249, 2016.

[3] S. Q. Li, H. L. Ji, and J. H. Qiu, "Active disturbance rejection controller based on state estimation error compensation for smart piezoelectric structure," *Journal of Mechanical Engineering*, vol. 48, no. 5, pp. 34–42, 2012.

[4] B. Siciliano and W. J. Book, "A singular perturbation approach to control of lightweight flexible manipulators," *International Journal of Robotics Research*, vol. 7, no. 4, pp. 79–90, 1988.

[5] J. Lin and F. L. Lewis, "Two-time scale fuzzy logic controller of flexible link robot arm," *Fuzzy Sets and Systems*, vol. 139, no. 1, pp. 125–149, 2003.

[6] X. Y. Yu and L. Chen, "Singular perturbation adaptive control and vibration suppression of free-flying flexible space manipulators," *Proceedings of the Institution of Mechanical Engineers Part C: Journal of Mechanical Engineering Science*, vol. 229, no. 11, pp. 1989–1997, 2015.

[7] Q.-X. Jia, X. Deng, M. Chu, and F.-J. Huang, "The composite control of dynamic switching sliding mode and optimal of one-link flexible manipulators," *Journal of Beijing University of Posts and Telecommunications*, vol. 36, no. 4, pp. 50–54, 2013.

[8] K. D. Dhuri and P. Seshu, "Piezo actuator placement and sizing for good control effectiveness and minimal change in original system dynamics," *Smart Materials and Structures*, vol. 15, no. 6, pp. 1661–1672, 2006.

[9] Z.-C. Qiu, X.-M. Zhang, H.-X. Wu, and H.-H. Zhang, "Optimal placement and active vibration control for piezoelectric smart flexible cantilever plate," *Journal of Sound and Vibration*, vol. 301, no. 3–5, pp. 521–543, 2007.

[10] S. Leleu, H. Abou-Kandil, and Y. Bonnassieux, "Piezoelectric actuators and sensors location for active control of flexible structures," *IEEE Transactions on Instrumentation and Measurement*, vol. 50, no. 6, pp. 1577–1582, 2001.

[11] Y. W. Yang, Z. L. Jin, and C. K. Soh, "Integrated optimal design of vibration control system for smart beams using genetic algorithms," *Journal of Sound and Vibration*, vol. 282, no. 3–5, pp. 1293–1307, 2005.

[12] A.-C. Lee and S.-T. Chen, "Collocated sensor/actuator positioning and feedback design in the control of flexible structure system," *Journal of Vibration and Acoustics, Transactions of the ASME*, vol. 116, no. 2, pp. 146–154, 1994.

[13] K. R. Kumar and S. Narayanan, "The optimal location of piezoelectric actuators and sensors for vibration control of plates," *Smart Materials and Structures*, vol. 16, no. 6, pp. 2680–2691, 2007.

[14] J. J. Zhang, L. L. He, and E. C. Wang, "Active vibration control of piezoelectric intelligent structures," *Journal of Computers*, vol. 5, no. 3, pp. 4184–4188, 2010.

[15] G. L. C. M. Abreu, J. F. Ribeiro, and V. Steffen Jr., "Experiments on optimal vibration control of a flexible beam containing piezoelectric sensors and actuators," *Shock and Vibration*, vol. 10, no. 5-6, pp. 283–300, 2003.

[16] H. Waisman and H. Abramovich, "Variation of natural frequencies of beams using the active stiffening effect," *Composites Part B: Engineering*, vol. 33, no. 6, pp. 415–424, 2002.

[17] C. Spier, J. Bruch, J. M. Sloss, S. Adali, and I. S. Sadek, "Placement of multiple piezo patch sensors and actuators for a cantilever beam to maximize frequencies and frequency gaps," *Journal of Vibration and Control*, vol. 15, no. 5, pp. 643–670, 2009.

[18] S. J. Bai, P. Ben-Tzvi, and Q. K. Zhou, "Dynamic modeling of a rotating beam having a tip mass," in *Proceedings of the IEEE International Workshop on Robotic and Sensors Environments*, pp. 52–57, Ottawa, Canada, October 2008.

[19] L. Q. Du, Y. H. Yan, and D. J. Wang, "The sense-actuate model of intelligent beam structures," *Chinese Journal of Applied Mechanics*, vol. 17, no. 2, pp. 114–117, 2000.

[20] D. Sun, J. K. Mills, J. Shan, and S. K. Tso, "A PZT actuator control of a single-link flexible manipulator based on linear velocity feedback and actuator placement," *Mechatronics*, vol. 14, no. 4, pp. 381–401, 2004.

[21] X. X. Yang and S. S. Ge, "Dynamics and tracking control for a free-flying space robot with rigid-flexible links," in *Proceedings of the IEEE International Conference on Information and*

Automation (ICIA '14), pp. 394–399, IEEE, Hailar, China, July 2014.

[22] K. Lochan, B. K. Roy, and B. Subudhi, "SMC controlled chaotic trajectory tracking of two-link flexible manipulator with PID sliding surface," *IFAC-PapersOnLine*, vol. 49, no. 1, pp. 219–224, 2016.

[23] A. E. Phillips, *A study of advanced modern control techniques applied to a twin rotor MIMO system [Ph.D. thesis]*, Rochester Institute of Technology, 2014.

[24] J.-J. Wei, Z.-C. Qiu, J.-D. Han, and Y.-C. Wang, "Experimental comparison research on active vibration control for flexible piezoelectric manipulator using fuzzy controller," *Journal of Intelligent and Robotic Systems*, vol. 59, no. 1, pp. 31–56, 2010.

[25] M. A. Ahmad, M. Z. M. Tumari, and A. N. K. Nasir, "Composite Fuzzy Logic control approach to a flexible joint manipulator," *International Journal of Advanced Robotic Systems*, vol. 10, article A55, 2013.

[26] J. K. Liu, *Advanced PID Control and MATLAB Simulation*, Publishing House of Electronics Industry, 2nd edition, 2004.